SPATIO-TEMPORAL CONSTRAINTS FOR EMISSIVITY AND SURFACE TEMPERATURE RETRIEVAL: PRELIMINARY RESULTS AND COMPARISONS FOR SEVIRI AND IASI OBSERVATION

Marilena Amoroso[1], Italia De Feis[2], Guido Masiello[1],
Carmine Serio[1], Sara Venafra[1], and Philip Watts[3]

1. University of Basilicata, School of Engineering, Potenza, Italy;
   marilena.amoroso(at)libero.it, {guido.masiello / carmine.serio /
   sara.venafra}(at)unibas.it
2. Istituto per le Applicazioni del Calcolo "M. Picone" (CNR), Napoli,
   Italy; i.defeis(at)iac.cnr.it
3. EUMETSAT, Darmstadt, Germany; philip.watts(at)eumetsat.int

ABSTRACT

Infrared instrumentation on geostationary satellites is now rapidly approaching the spectral quality and accuracy of modern sensors flying on polar platforms. Currently, the core of EUMETSAT geostationary meteorological programme is the Meteosat Second Generation (MSG). However, EUMETSAT is preparing for the Meteosat Third Generation (MTG). The capability of geostationary satellites to resolve the diurnal cycle and hence to provide time-resolved sequences or times series of observations is a source of information which could suitably constrain the derivation of geophysical parameters.

Nowadays, also because of lack of time continuity, when dealing with observations from polar platforms, the problem of deriving geophysical parameters is normally solved by considering each single observation as independent of past and future events. For historical reason, the same approach is currently pursued with geostationary observations, which are still being dealt with as they were with polar observations.

In this study we show some preliminary results on emissivity and surface temperature retrieval for SEVIRI observations, using the Kalman filter methodology (KF) and compare the retrievals with those obtained using IASI observations co-localized with SEVIRI ones using the times accumulation approach (Optimal Estimation OE). The Sahara desert was chosen as target area, and both SEVIRI and IASI data (infrared radiances and cloud mask) were acquired. The time period considered is that of July 2010 (the whole month). ECMWF analyses for the same date and target area have also been acquired, which comprise T_s, $T(p)$, $O(p)$, $Q(p)$ for the canonical hours 0:00, 6:00, 12:00 and 18:00. Moreover, for the purpose of developing a suitable background for emissivity, the Global Infrared Land Surface Emissivity database developed at CIMSS, University of Wisconsin, derived by MODIS observations was used and was available from the year 2003 till 2011.

Concerning the performance of the two methodologies, the retrieval of skin temperature is almost equivalent. The agreement between OE and KF is fairly good if compared with ECMWF analysis for sea surface, while for land surface, OE and KF agree fairly well with ECMWF during the night, but at midday ECMWF shows a cold bias of 10 K and more. For emissivity the comparison with the UW/BFEMIS database for the same date and location is fairly good for both methods.

INTRODUCTION

Nowadays the retrieval of geophysical parameters from satellite observations largely relies on *a priori* information, which is derived from climatology and/or models for Numerical Weather Prediction. Thus, the retrieval problem can be efficiently analysed within the broad context of data assimilation, which is indeed the paradigm of the many seemingly different methods, which have been developed over the past years, such as Optimal Estimation and Kalman Filter which end up with the same formal solution as far as the estimate of geophysical parameters is concerned.

The present study wants to define a suitable retrieval methodology for the infrared channels of the Meteosat Second Generation (MSG) SEVIRI (Spinning Enhanced Visible and Infrared Imager), identifying a retrieval case of study for surface emissivity and temperature in order to exemplify the strategy of how to consider the spatio-temporal variability of the data. Finally, these retrievals are compared with IASI (Infrared Atmospheric Sounding Interferometer) ones.

Both methodologies (OE and KF) were applied to SEVIRI data in order to retrieve geophysical parameters, obtaining similar results, see, for example, Figure 70 and relative text in Section 10.2 of (1). For this reason a Kalman filter was used for SEVIRI since the instrument, being geostationary, provides data every 15 minutes considering in this way the time-evolution of the instrument. Optimal estimation was used for IASI.

Spatial variability is still to be externally included through a suitable definition of the background covariance matrix, which inevitably increases the dimension of the state vector. Thus, in the end the problem is fundamentally one of data-dimension reduction. To date, this problem has mostly been dealt with suitable orthogonal transforms, which can allow us to compress much of the data and state vector information in few coefficients of the expansion.

In this paper the data space and the methods used to apply spatio-temporal constraints for surface emissivity and temperature retrievals is described, followed by an application to real SEVIRI observations and results concerning daily maps of emissivity and temperature. Conclusions and recommendations are taken in respect of the METEOSAT Third Generation (MTG) Infrared Sounder.

METHODS

IASI has been developed in France by the Centre National d'Etudes Spatiales (CNES) and is flying on board the Metop-A (Meteorological Operational Satellite) platform, the first of three satellites of the European Organization for the Exploitation of Meteorological Satellite (EUMETSAT) European Polar System (EPS). Its main objective is to provide suitable information on temperature and water vapour profiles. The instrument has a spectral coverage extending from 645 to 2,760 cm^{-1}, which, with a sampling interval of $\Delta\sigma$ = 0.25 cm^{-1}, gives 8,461 channels for each single spectrum.

Data samples are taken at intervals of 25 km along and across tracks, each sample having a minimum diameter of about 12 km. With a swath width on Earth's surface of about 2,000 kilometers, global coverage is achieved within 12 hours, during which the instrument records about 650,000 spectra. Further details on IASI and its mission objectives can be found in (2).

The retrieval of surface and atmospheric parameters from IASI spectral radiances is carried out with a package that we call ϕ-IASI, whose methodological aspects and validation have been described in many papers (3,4,5,6,7,8,9,10,11,12,13,14,15,16,17).

The SEVIRI instrument has instead eight infrared channels: 13.4 (746.30), 12.0 (833.33), 10.8 (925.90), 9.7 (1030.9), 8.7 (1149.40), 7.3 (1369.9), 6.2 (1612.9), 3.9 (2564.10) μm (cm^{-1}), respectively. We have not used the last channel for different reasons which can add a potential large bias, such as channel 3.9 μm, which is too broad and is contaminated from solar emission in daytime, etc. The time resolution of the data is 15 min, whereas each pixel has a size of 3×3 km^2. In order to obtain a simplified derivation of the radiance (σ-SEVIRI), two types of reflections are used: specular and Lambertian reflection. The forward model σ-SEVIRI is derived from the σ-IASI monochromatic radiative transfer for fast computation of spectral radiance and its derivatives (Jacobian) with respect to a given set of geophysical parameters.

The methodologies adopted for the retrieval of geophysical parameters are described below.

Optimal estimation

The Optimal Estimation (OE) allows us to accumulate the observations during the day, in order to consider the time-evolution and then to introduce time constraints. For its implementation various strategies have been used with the aim to perform the retrieval, such as the use of different time slot widths considering the accumulation of observations and the development of static background

covariance matrices with fully dependent/independent or correlated state vectors, for either temperature or emissivity. Data assimilation (18) provides a good paradigm for the many methods which are reviewed here. In particular the methods that consider the a-priori covariance as a static application data, that is Rodgers's Optimal Estimation (19), 1D to 3D variational analysis (20,21), and the Maximum Likelihood Estimation approach are formally equivalent (17). Therefore, in reviewing the basic aspects of the retrieval problem with a static *a priori*, we approach the issue from the variational perspective, since it has a more straightforward generalization to the fourth time-dimension. In this way our retrieval problem is comparable to a variational analysis in which a suitable estimation of the state vector is obtained by minimizing the form shown in Eq. (1):

$$\min_{\mathbf{v}} \left[\frac{1}{2} \left(\mathbf{R} - F(\mathbf{v}) \right)^T \mathbf{S}_\varepsilon^{-1} \left(\mathbf{R} - F(\mathbf{v}) \right) + \frac{1}{2} \left(\mathbf{v} - \mathbf{v_a} \right)^T \mathbf{S}_a^{-1} \left(\mathbf{v} - \mathbf{v_a} \right) \right] \tag{1}$$

where $\mathbf{R}$ is the radiance vector, F is the forward model function, $\mathbf{v}$ is the atmospheric state vector of size N, $\mathbf{v_a}$ is the atmospheric background state vector of size N, $\mathbf{S}_\varepsilon$ is the observational covariance matrix of size $M \times M$, and $\mathbf{S_a}$ is the background covariance matrix of size $N \times N$.

It is assumed that the variability of emissivity is much slower than that of surface temperature: the emissivity is considered constant on the time span, while the surface temperature can vary free with time.

Kalman filter

The Kalman filter (KF) is a linear filter developed by Kalman and Bucy (22,23). This filter is summarized with the couple of equations represented in Eq. (2), which refers to as the observation equation and the state equation respectively.

$$\begin{cases} \mathbf{R_t} = F(\mathbf{v_t}) + \boldsymbol{\varepsilon_t} \\ \mathbf{v_{t+1}} = \mathbf{H}\mathbf{v_t} + \boldsymbol{\eta_t} \end{cases} \tag{2}$$

In Eq. (2), $\mathbf{H}$ is a linear operator, $\boldsymbol{\varepsilon_t}$ and $\boldsymbol{\eta_t}$ are both independent noise terms of the state vector. It is very important to know that the analysis of the formal solution does not depend on the data at previous time but only on that at time t (Markov property (24)). We have used a simple persistence model for emissivity and surface temperature since the information content of the observations is very high, thus a simplistic state equation can represent the data very well. For the surface temperature retrieval on land we cannot use the model just mentioned, but an autoregressive model of the second order is implemented, where the coefficients are obtained directly from SEVIRI observations. In fact, a simple persistence model cannot reproduce the daily cyclic behaviour expected in condition of clear sky for land surface, while it is a fair model for sea surface, where thermal inertia of water strongly damps the effect of the solar cycle.

The Kalman filter is able to sequentially process the observations, reducing the dimensionality of the retrieval system and has also the capability of dealing with unequally spaced times, allowing the jumping over cloudy periods in order to process only clear sky observations, without the need to re-initialize the filter. This is an advantage of this methodology with respect to Optimal Estimation. This is the reason why we preferred to adopt this methodology to SEVIRI observations, also because we take account for time-continuity of SEVIRI data in this way.

Otherwise we dealt with OE for the retrieval of geophysical parameters from IASI data, due to the polar orbit type of the instrument with two observations per day at 09:00 AM and 08:00 PM.

Further details of these methodologies are described in (25).

Application to real SEVIRI observation and IASI-SEVIRI spatial co-location

Target area

The target area extends from 15°W to 10°E longitude and from 25°N to 45°N latitude (Figure 1). This selection has been made in order to obtain monthly maps for emissivity and surface temperature over the whole target area for which SEVIRI observations (Meteosat 9 high rate SEVIRI level

1.5 image data) have been acquired for the whole month of July 2010. An example of monthly SEVIRI emissivity retrieval, obtained with the Kalman filter methodology, is represented in Figure 2. In this figure one can see the large variability in the emissivity existent especially in the desert areas, more evident in the 8.7 µm channel, due to the fact that these areas are rich in quartz.
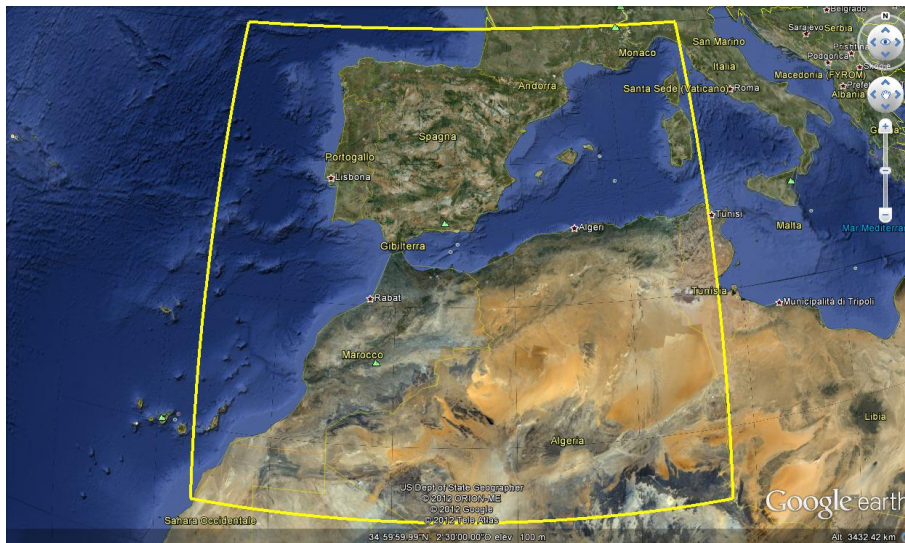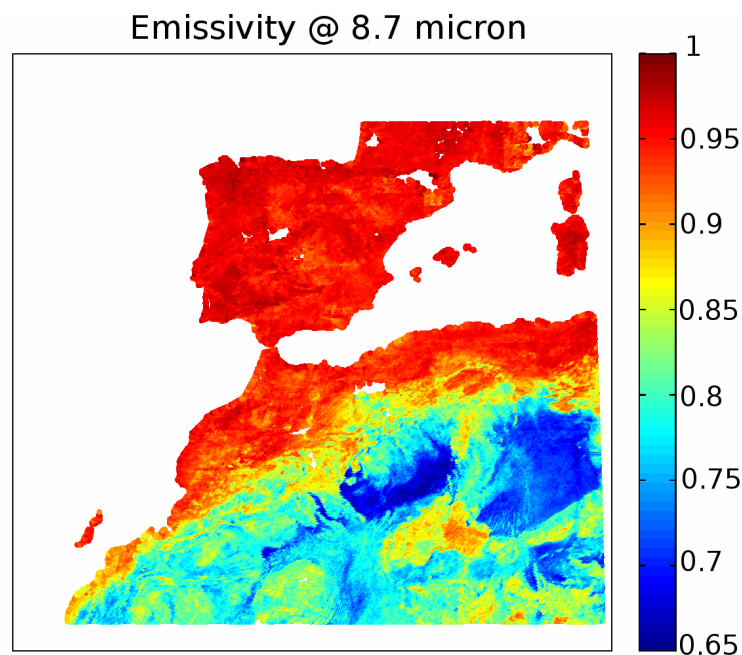

Figure 1: Target area.

Figure 2: Monthly SEVIRI emissivity retrieval at 8.7 µm (July 2010).

A comparison between the results obtained from IASI and SEVIRI has been made for three target areas, in Spain, in the Sahara desert in the middle of Algerian desert, and in the ocean near the South of Sardinia Island, to consider the presence of vegetation and bare soil, desert sand and sea. For the sake of brevity we focus our attention on the desert region of Ouargla Province, Algeria, which extends from 4° to 8°E and from 29° to 33°N, in order to show the comparisons between emissivity and surface temperature for SEVIRI and IASI at SEVIRI space and time resolution.

Ancillary data and background

Ancillary information about the atmospheric component has also been acquired and used as a first guess for the surface and atmospheric parameters. For this purpose ECMWF analyses have been utilized, that is the state vector composed of T_s, $T(p)$, $O(p)$, $Q(p)$ (surface temperature, atmospheric

profiles of temperature, ozone and water vapour, respectively) for the canonical hours 0:00, 6:00, 12:00 and 18:00, with a horizontal spatial resolution of 0.5 × 0.5 degrees. In each ECMWF grid box there are on average ≈200 SEVIRI pixels. A linear interpolation of this state vector has been made on the temporal MSG resolution grid (acquisition each 15 minutes, for a total of 96 daily time points).

In order to build up the emissivity background, we have used the emissivity database of the Global Infrared Land Surface Emissivity (UW/BFEMIS: http://cimss.ssec.wisc.edu/iremis/) developed at CIMSS, University of Wisconsin (26). In doing so, we have not used July 2010, left for checking/validation. This database was derived by MODIS observations and was available from the year 2003 till 2011. The emissivity was made available on a monthly basis, at ten wavelength points (or hinge points) on a 0.05 × 0.05 degree grid. The wavelengths are 3.6, 4.3, 5.0, 5.8, 7.6, 8.3, 9.3, 10.8, 12.1, and 14.3 μm. The emissivity cannot be straightly interpolated to the SEVIRI channels because of the different spectral response function between MODIS and SEVIRI.

This problem has been handled by developing a suitable software, which first extrapolates the low spectral resolution emissivity spectrum to the IASI wavenumber range, and second, through convolution with the SEVIRI spectral response, to the SEVIRI channels (Figure 3). In this way the emissivity a-priori covariance matrix has been estimated for each point of the SEVIRI grid on the target area, useful to introduce spatial variability for the Optimal Estimation and Kalman filter methodologies shown below.
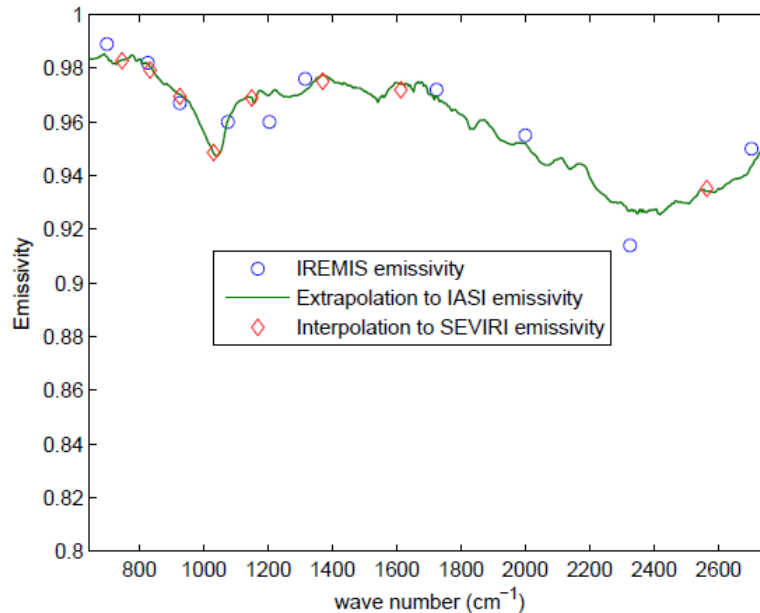

Figure 3: From UW/BFEMIS to SEVIRI emissivity, passing through IASI.

IASI-SEVIRI spatial co-location

In order to correctly compare the SEVIRI retrievals with IASI ones, we have co-located SEVIRI pixels with IASI footprints spatially. In detail, the IASI emissivity spectrum has been convolved to SEVIRI channels by means of the following equation:

$$\varepsilon^S(\sigma_{ch}) = ISRF(\sigma_{ch}, \sigma) \cdot \varepsilon^I(\sigma) \tag{3}$$

where ε^S is the IASI retrieved emissivity to SEVIRI channels, ε^I is the IASI emissivity to IASI channels and ISRF are the Instrument Spectral Response Function of SEVIRI MSG FM2 in correspondence to infrared channels. Figure 4 shows the IASI emissivity retrieved on the SEVIRI ISRF. For the emissivity retrieval we used the 8.7, 10.8, and 12 μm channels. It is evident that at 1149.4 cm−1 there is a spatial variability in the emissivity, which follows the distribution of the richer quartz sand across the desert.

In the box of interest we have also 2 Metop orbits, at 9 AM and at 8 PM, for a total of about 10 IASI scan lines. For every day there are more than 400 IASI footprints (200 daytime, 200 nighttime).
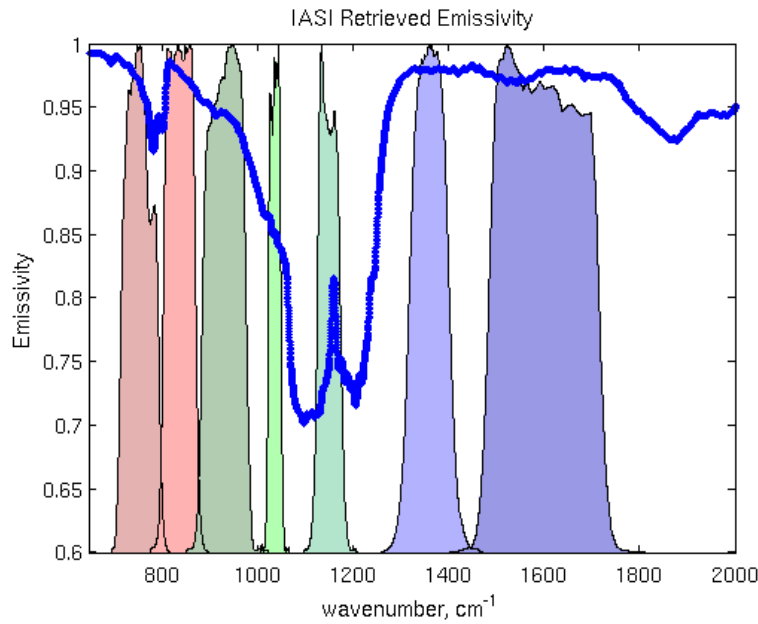
Figure 4: IASI emissivity spectrum on the SEVIRI channels.

RESULTS

The Kalman filter (for SEVIRI) and the Optimal Estimation (for IASI) methods have been applied to the whole month of July 2010. SEVIRI observations for the target area shown in Figure 1 are computed at SEVIRI time (15 min) and spatial resolution and then averaged to form daily and monthly maps.

The UW/BFEMIS database has been used to build up the emissivity background, all but year 2010 used for comparison with the retrieval products. We have been processed only clear sky observations, qualified according to the SEVIRI operational cloud mask (27,28,29,30). In particular, we want to compare IASI-SEVIRI retrievals in 2010, July, 10, AM & PM; 2010, July, 4, AM for emissivity and in whole July 2010 for skin temperature. In Fig. 5 the IASI derived SEVIRI channels emissivity is represented for 2010, July, 10, AM & PM.
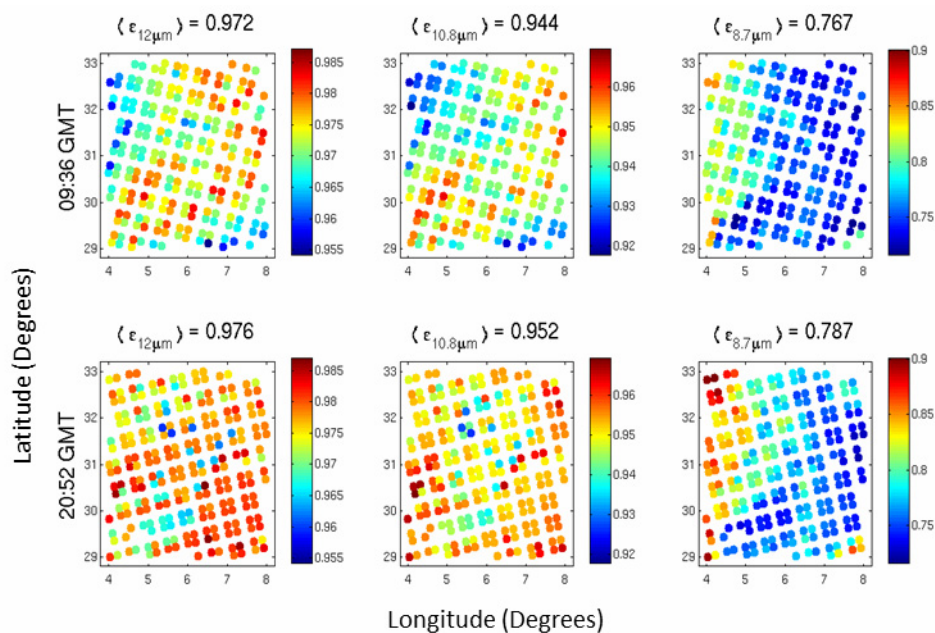

Figure 5: IASI emissivity retrievals (OE) on SEVIRI channels (8.7, 10.8 and 12 µm) for 2010, July, 10, AM & PM.

In Fig. 6 a) and b) there are the comparisons between IASI (in circles) and SEVIRI both for emissivity and skin temperature in 2010, July, 10, AM and PM, respectively.
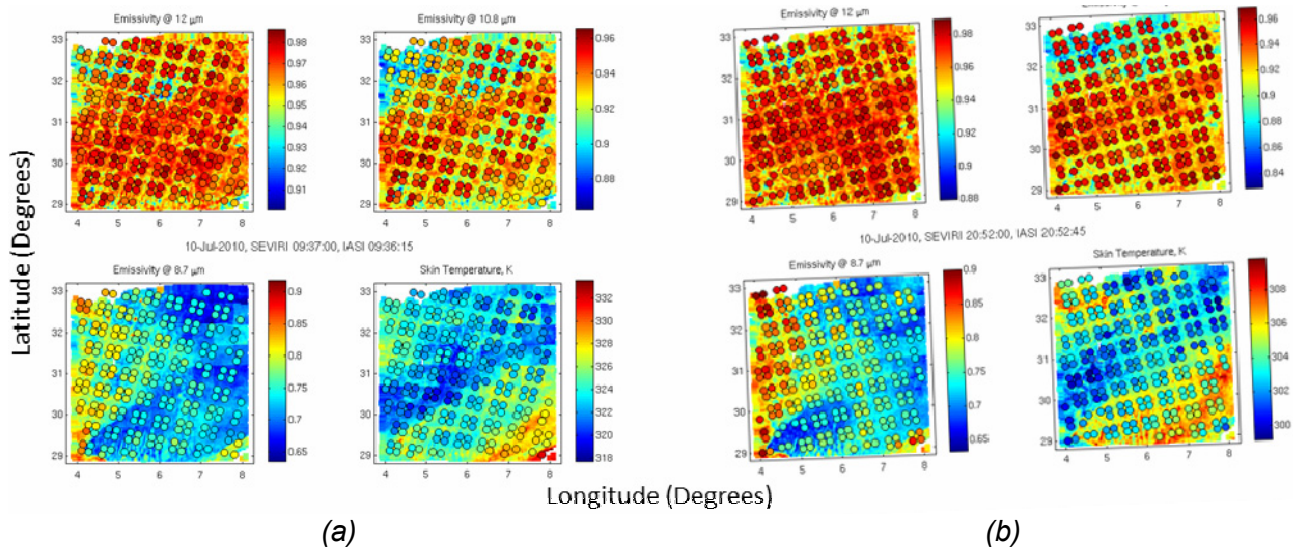

(a)   *(b)*

Figure 6: Comparison between IASI (OE) and SEVIRI (KF) retrievals in 2010, July, 10, AM (a) and PM (b).

For Figure 6 (a) 237 IASI spectra have been used, for (b) 246. In Figure 7, we present the histogram of differences for emissivity and skin temperature SEVIRI-IASI for the same data.
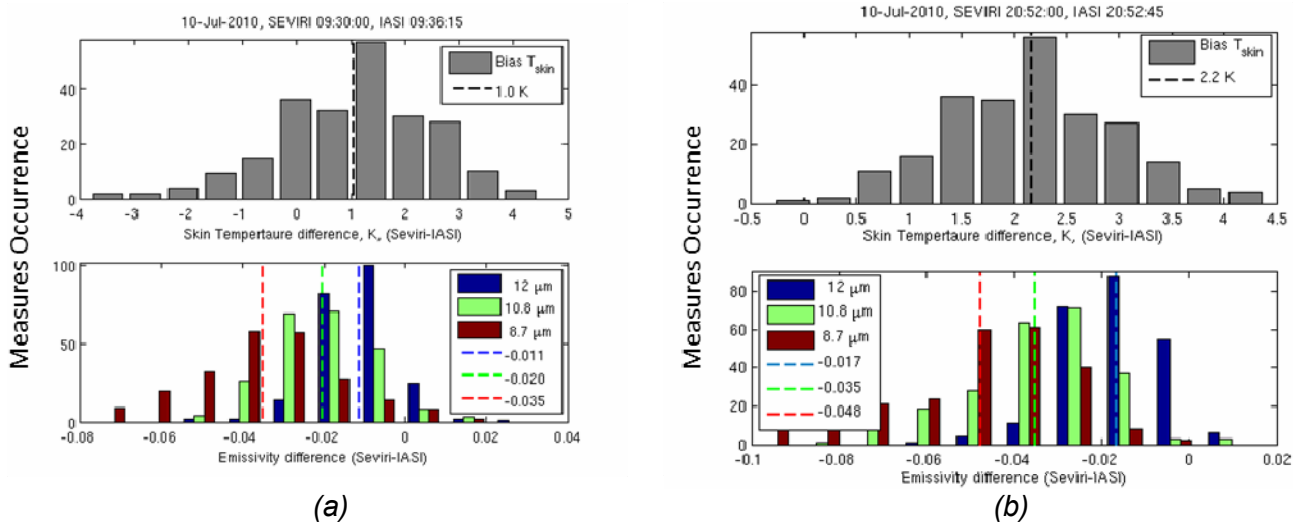

(a)   *(b)*

Figure 7: Histogram of differences between SEVIRI (KF) and IASI (OE) for skin temperature and emissivity in 2010, July 10, AM (a) and PM (b).

In order to obtain these comparisons, we have averaged the SEVIRI retrievals (3×3 km^2) within the IASI pixel (12×12 km^2). As depicted in Figure 7, the mean difference between SEVIRI-IASI skin temperature is about 1 K at daytime and 2.2 K at nighttime, while for emissivity comparison we find a mean difference of 0.02 and 0.035 at 10.8 μm in the daytime and nighttime, respectively.

These results are very encouraging and the situation improves for 2010, July 4, AM with a mean difference of 0.9 K for skin temperature and of about zero for emissivity at 10.8 μm, as shown in Figure 8 (b). The number of IASI spectra used for these retrievals is 123. Similar results have been obtained for the other areas of interest.

A very good agreement is also achieved comparing IASI and SEVIRI skin temperature with ECMWF profiles for the whole month of July 2010 (Figure 9).
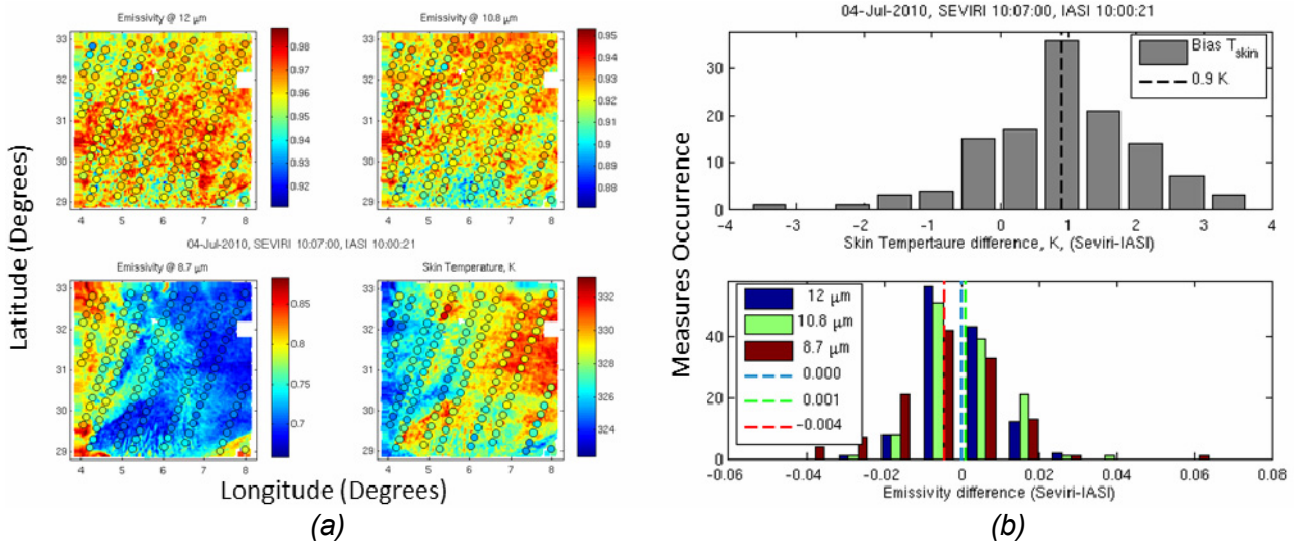
Figure 8: Comparison between IASI and SEVIRI retrievals in 2010, July 4, AM (a) and relative histograms of difference for skin temperature and emissivity.
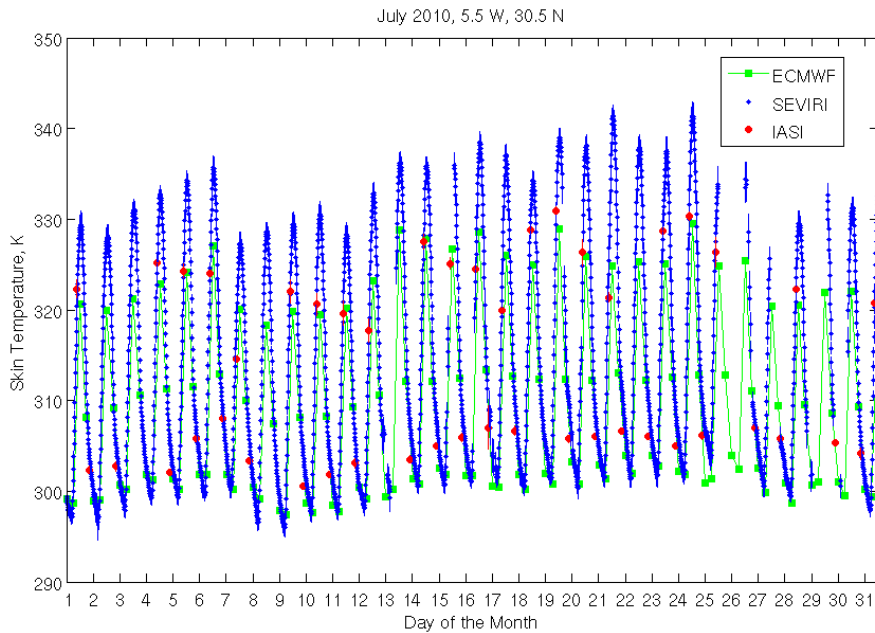

Figure 9: Daily skin temperature for ECMWF (green), SEVIRI (blue) and IASI (red) in the whole month of July 2010.

As shown in Figure 9, for land surface, OE (IASI) and KF (SEVIRI) agree fairly well with ECMWF for nighttime observations, but at midday ECMWF shows a cold bias, which can achieve 10 K and more.

This problem can be justified by the emissivity used for the calculation, extracted from the UW/BFEMIS database. It is interesting to note the large sensitivity of the skin temperature on emissivity.

Our emissivity retrieval, obtained with the KF methodology and applied to SEVIRI data, differs from the UW/BFEMIS values by less than 1%, however, it causes differences of up to 2-3 K again in the hottest part of the day (1,25). In passing, the statistical method seems to give very nice results for Spain. For the Sahara desert the temperature is largely underestimated at midday. Thus, ECMWF analyses underestimate the maximum temperature in the desert areas by more than 10 K, while the comparison between IASI (OE) and SEVIRI (KF) retrievals show a very good agreement (1,25).

Furthermore, we have demonstrated that there is a variability of emissivity with the diurnal cycle in the desert areas (Fig. 10). This case study has been analysed by Li et al. (31) which we want to complement and to stress that the observed day/night emissivity variation is due to soil moisture.
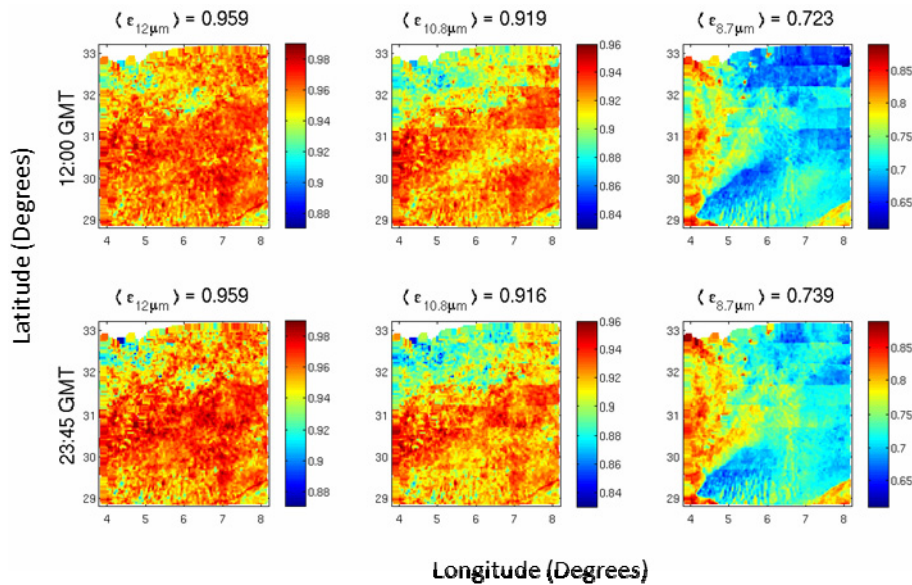

Figure 10: SEVIRI emissivity variability with the diurnal cycle in the Sahara desert.

This variability is more evident at 8.7 µm: The minimum of the emissivity is exactly at midday and it is significant with the well-known diurnal cycle of soil moisture (32,33), as shown in Figure 11.

During the dry season, the amplitude of the soil moisture cycle is normally 1-2%. Concerning the effect of soil moisture on rich quartz sand, we conclude that the amplitude of the soil moisture is enough to yield diurnal variations of the emissivity at 8.7 µm as large as 0.04 (34).
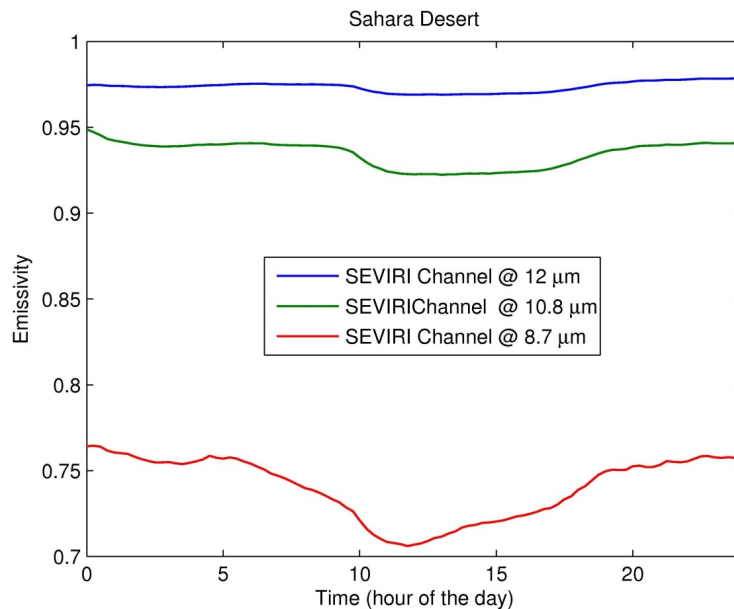

Figure 11: SEVIRI retrieved day/night emissivity versus diurnal cycle in the Sahara desert.

This day/night emissivity variability has also been observed in an IASI retrieved emissivity spectrum, as depicted in Figure 12. In red we have drawn the IASI emissivity spectra averaged over 229 footprints recorded during daytime (09:36 GMT), while in blue the IASI emissivity spectra averaged over 205 footprints recorded during nighttime (20:52 GMT) are illustrated.
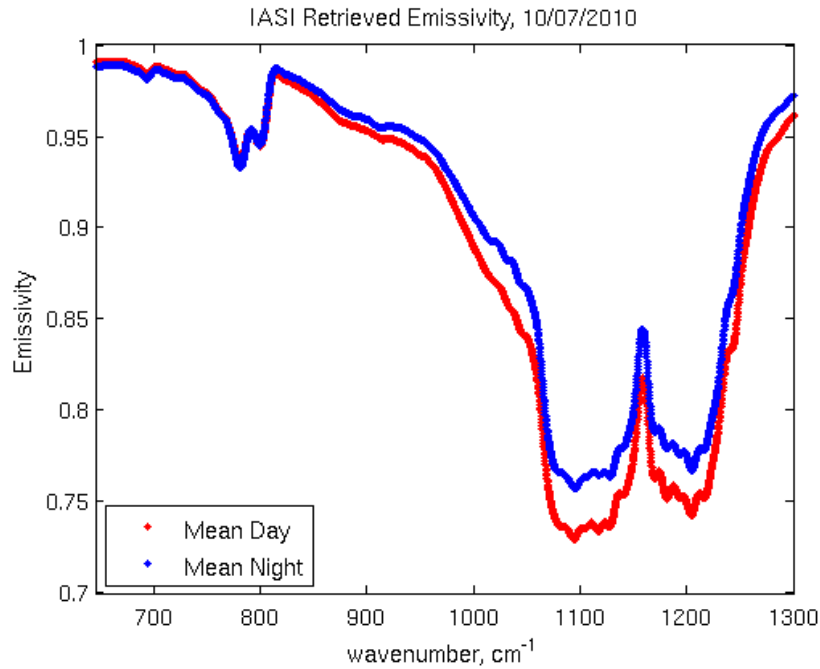
Figure 12: IASI retrieved emissivity spectra for daytime (red) and nighttime (blue) for 10 July 2010.

In detail, Figure 13 shows the IASI retrieved emissivity variability at 8.7 µm for the whole month of July 2010. Remembering that IASI is flying on a polar platform, we have two data per day, one at 09:00 AM in descending orbit at daytime (blue dots) and the other at 08:00 PM in ascending orbit at nighttime (red dots). From this figure it is evident that during nighttime emissivity is systematically larger than that retrieved during daytime, which leads us to conclude that the only mechanism responsible for the day/night emissivity variation is the direct water vapour adsorption at the surface (34).
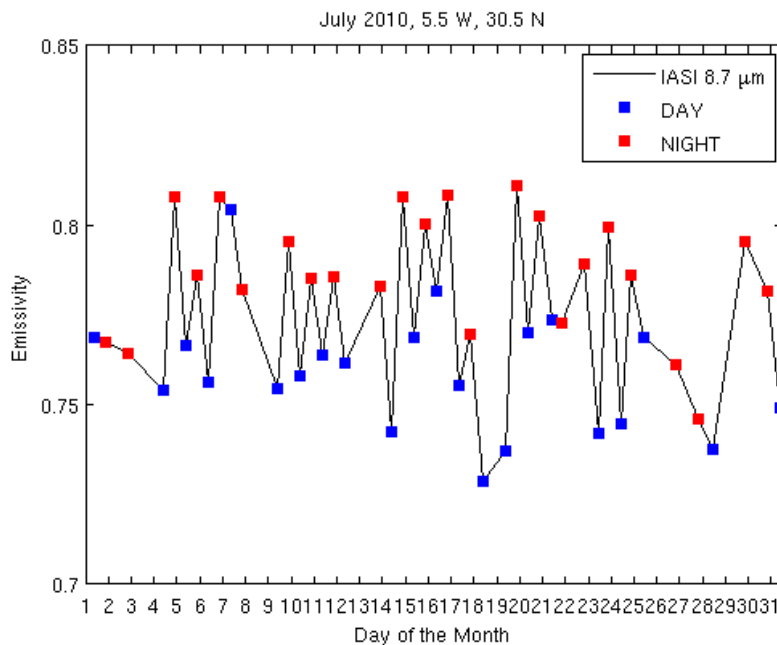

Figure 13: IASI retrieved emissivity spectrum for daytime (blue) and nighttime (red) at 8.7 µm versus diurnal cycle for the whole July 2010.

CONCLUSIONS

We have reviewed variational and sequential optimal estimation schemes with the objective to apply them to SEVIRI infrared observations. Specific algorithms have been developed and implemented for the two basic parameters, skin temperature and emissivity.

Concerning the performance of the two applied methodologies, as far as the retrieval of skin temperature is concerned, OE and KF are almost equivalent, although a slight bias (of order of 1 K) between the two still persists even on monthly averages. For sea surface we have observed a good agreement between OE (for IASI) and KF (for SEVIRI) retrievals with ECMWF analyses, while for land surface this correspondence is fairly good during nighttime, but at midday there is a bias of 10 K largely due to ECMWF analyses underestimation.

For emissivity, the comparison with the UW/BFEMIS database for the same date and location is fairly good. OE stays closer to UW/BFEMIS, whereas KF seems to add information independent of that contained in the UW/BFEMIS database.

Altogether, the Kalman filter has to be preferred to Optimal Estimation in order to take advantage of time continuity and constraint for the retrieval of surface temperature and emissivity from SEVIRI data. In fact, with KF it is possible to process time sequences of data points without affecting the dimensionality of the retrieval problem. Even though skin temperature is better represented by a deterministic second-order difference equation, because it is governed by the diurnal cycle, we recommend to use a persistence model for both sea and land surfaces. In fact, KF can accommodate the state equation or model for the process also when this equation is inherently inadequate to describe the real-world phenomenon. Our confidence about the state equation is accommodated within scheme through a stochastic variance term which can trade-off between data and model.

It is assumed that after a training/validation phase, including situations of abrupt changes in surface parameters and/or radiances (e.g. rainfall, cloudiness, weather events) and using ground truth data, the Kalman approach for the retrieval of $T_s-\varepsilon$ from SEVIRI window channels could become operational. It is therefore planned to build a full disk SEVIRI emissivity database.

For the problem of deriving a suitable background for emissivity for land surface it is definitely recommended to use the UW/BFEMIS database.

In respect of MTG-IRS or geostationary high spectral resolution infrared instruments, one important issue is how to include atmospheric parameters within the retrieved state vector. In this case, a better strategy would be to use a persistence model at each layer and introduce inter-layer correlation through the definition of a proper background as it is done, e.g., with IASI in the context of one-dimensional data assimilation.

ACKNOWLEDGEMENTS

REFERENCES

1   Serio C, G Masiello, M Amoroso, S Venafra, U Amato & I De Feis, 2012. Study on space-time constrained parameter estimation from geostationary data. EUMETSAT Contract EUM/CO/11/4600000996/PDW, Final Report, 137 pp. (last date accessed: 25 Oct 2013)

2   Hilton F, R Armante, T August, C Barnet, A Bouchard, C Camy-Peyret, V Capelle, L Clarisse, C Clerbaux, P F Coheur, A Collard, C Crevoisier, G Dufour, D Edwards, F Faijan, N Fourrié, A Gambacorta, M Goldberg, V Guidard, D Hurtmans, S Illingworth, N Jacquinet-Husson, T Kerzenmacher, G Klaes, L Lavanant, G Masiello, M Matricardi, A Mc-Nally, S Newman, E Pavelin, S Payan, E Péquignot, S Peyridieu, T Phulpin, J Remedios, P Schlüssel, C Serio, L Strow, C

Stubenrauch, J Taylor, D Tobin, W Wolf & D Zhou, 2012. Hyperspectral Earth Observation from IASI: Four years of accomplishments. Bulletin of the American Meteorological Society, 93: 347-370

3   Amato U, V Cuomo, I De Feis, F Romano, C Serio & H Kobayashy, 1999. Inverting for geophysical parameters from IMG radiances. IEEE Transactions on Geoscience and Remote Sensing, 37: 1620-1632, 1999

4   Lubrano A M, C Serio, S A Clough & H Kobayashy, 2000. Simultaneous inversion for temperature and water vapor from IMG radiances. Geophysical Research Letters, 27: 2533-2536

5   Grieco G, G Masiello, M Matricardi, C Serio, D Summa & V Cuomo, 2007. Demonstration and validation of the ϕ-IASI inversion scheme with NAST-I data. Quarterly Journal of the Royal Meteorological Society, 133(S3), 217-232

6   Amato U, A Antoniadis, I De Feis, G Masiello, M Matricardi & C Serio, 2009. Technical Note: Functional sliced inverse regression to infer temperature, water vapour and ozone from IASI data. Atmospheric Chemistry and Physics, 9: 5321-5330

7   Masiello G, C Serio, A Carissimo, G Grieco & M Matricardi, 2009. Application of φ-IASI to IASI: retrieval products evaluation and radiative transfer consistency. Atmospheric Chemistry and Physics, 9, 8771-8783

8   Grieco G, G Masiello & C Serio, 2010. Interferometric *vs* spectral IASI radiances: Effective data-reduction approaches for the satellite sounding of atmospheric thermodynamical parameters. Remote Sensing, 2(10), 2323-2346

9   Masiello G, M Amoroso, P Di Girolamo, C Serio, S Venafra & T Deleporte, 2012. IASI retrieval of temperature, water vapor and ozone profiles over land with ϕ-IASI package during the COPS campaign. Proceedings of the 9th International Symposium on Tropospheric Profiling (CETEMPS - University of L'Aquila, Italy) (last date accessed: 25 Oct 20123)

10   Amato U, M F Carfora, V Cuomo & C Serio, 1995. Objective algorithms for the aerosol problem. Applied Optics 34, 5442-5452

11   Amato U, D De Canditiis & C Serio, 1998. Effect of apodization on the retrieval of geophysical parameters from Fourier-Transform Spectrometers. Applied Optics, 37: 6537-6543

12   Amato U, G Masiello, C Serio & M Viggiano, 2002, The σ-IASI code for the calculation of infrared atmospheric radiance and its derivatives, Environmental Modelling & Software, 17(7): 651-667

13   Masiello G & C Serio, 2004. Dimensionality-reduction approach to the thermal radiative transfer equation inverse problem. Geophysical Research Letters, 31, L11105

14   Carissimo A, I De Feis & C Serio, 2005. The physical retrieval methodology for IASI: the δ-IASI code. Environmental Modelling & Software, 20(9): 1111-1126

15   Masiello G, M Matricardi & C Serio, 2011. The use of IASI data to identify systematic errors in the ECMWF forecasts of temperature in the upper stratosphere. Atmospheric Chemistry and Physics, 11, 1009-1021

16   Masiello G, C Serio & P Antonelli, 2011. Inversion for atmospheric thermodynamical parameters of IASI data in the principal components space. Quarterly Journal of the Royal Meteorological Society, 138(662): 103-117

17   Masiello C & C Serio, 2013. Simultaneous physical retrieval of surface emissivity spectrum and atmospheric parameters from Infrared Atmospheric Sounder Interferometer spectral radiances. Applied Optics, 52, 2428-2446

18   Wikle C K & L M Berliner, 2007. A Bayesian tutorial for data assimilation. Physica D, 230(1): 1-16

19   Rodgers C D, 2000. Inverse Methods for Atmospheric Sounding, Theory and Practice. Series on Atmospheric, Oceanic and Planetary Physics, Vol. 2 (World Scientific, Singapore)

20   Courtier P, 1997. Variational methods. Journal of the Meteorological Society of Japan, 75: 211-218

21   Talagrand O, 1997- Assimilation of observations, an introduction. Journal of the Meteorological Society of Japan, 75: 191-209

22   Kalman R E, 1960. A new approach to linear filtering and prediction problems. Journal of Basic Engineering, 82(1): 35-45

23   Kalman R E & R S Bucy, 1961. New results in linear filtering and prediction theory. Transactions of the ASME - Journal of Basic Engineering, 83, 95-107

24   Nychka D & J L Anderson, 2008. Data Assimilation. Draft article for the Handbook on Spatial Statistics (National Center for Atmospheric Research, Boulder, CO, USA) 19 pp.

25   Masiello G, C Serio, I De Feis, M Amoroso, S Venafra, I F Trigo & P Watts, 2013. Kalman filter physical retrieval of geophysical parameters from high temporal resolution geostationary infrared radiances: the case of surface emissivity and temperature. Atmospheric Measurement Techniques, 6: 6873-6933, under review (last date accessed: 31. Oct 2013)

26   Borbas E E & B C Ruston, 2010. The RTTOV UWiremis IR land surface emissivity module. NWP SAF, EUMETSAT (last date accessed: 29 Oct 2010)

27   Serio C, A Lubrano, F Romano & H Shimoda, 2000. Cloud detection over sea surface by use of autocorrelation functions of upwelling infrared spectra in the 800-900 cm^{-1} window region. Applied Optics, 39: 3565-3572

28   Masiello G, M Matricardi, R Rizzi & C Serio, 2002. Homomorphism between cloudy and clear spectral radiance in the 800-900 cm^{-1} atmospheric window region. Applied Optics, 41: 965-973

29   Masiello G, C Serio & V Cuomo, 2004. Exploiting quartz spectral signature for the detection of cloud-affected satellite infrared observations over African desert areas. Applied Optics, 43: 2305-2315

30   Masiello G, C Serio & H Shimoda, 2003. Qualifying IMG tropical spectra for clear sky. Journal of Quantitative Spectroscopy & Radiative Transfer, 77: 131-148

31   Li Z, J Li, Y Li, Y Zhang, T J Schmit, L Zhou, M D Goldberg & W P Menzel, 2012. Determining diurnal variations of land surface emissivity from geostationary satellites. Journal of Geophysical Research, 117, D23302

32   Agam N & P R Berliner, 2004. Diurnal water content changes in the bare soil of a coastal desert. Journal of Hydrometeorology, 5: 922-933

33   Agam N & P R Berliner, 2006. Dew formation and water vapor adsorption in semi-arid environments: a review. Journal of Arid Environments, 65: 572-590

34   Masiello G, C Serio, S Venafra, I De Feis & E E Borbas, 2013. Diurnal variation in Sahara desert sand emissivity during the dry season from IASI observations. Journal of Geophysical Research, accepted article